CMS Physics Analysis Summary

Contact: cms-pag-conveners-heavyions@cern.ch 2024/11/22

Constraining nPDFs using dijet production in pPb collisions at 8.16 TeV with the CMS experiment

The CMS Collaboration

Abstract

The dijet pseudorapidity (η^{dijet}) distribution in proton-lead (pPb) collisions is sensitive to nuclear modifications of parton distribution functions (PDFs). Additionally, the measurement of the η^{dijet} dependence of the average transverse momenta of dijets provides a precise method for investigating the energy scale of partonic interactions and their momentum transfer dependence (Q^2). Previously published measurements of dijet production in pPb collisions at a center-of-mass collision energy per nucleon pair of $\sqrt{s_{\text{NN}}} = 5.02$ TeV were used to constrain nuclear PDF fits based on next-to-leading order calculations. Here, a new measurement of dijet distributions using pPb collision data collected at a higher energy of 8.16 TeV is reported. The data, recorded by the CMS experiment at the LHC, correspond to an integrated luminosity of 174.6 nb^{-1}. The η^{dijet} distributions are measured for multiple dijet average transverse momentum $p_{\text{T}}^{\text{ave}}$ intervals from 50 to 500 GeV.

1 Introduction

The nuclear parton distribution function (nPDF) extends the concept of parton distribution functions (PDFs) from free protons to complex nuclei. It characterizes the probability of finding a parton (quark or gluon) within a nucleus that carries a fraction of the nucleon's momentum, x, at a particular resolution scale, Q^2. The nPDF encapsulates various nuclear effects, including shadowing at low x ($x \lesssim 10^{-2}$), antishadowing at intermediate x ($10^{-2} \lesssim x \lesssim 10^{-1}$), the EMC effect at high x ($10^{-1} \lesssim x \lesssim 0.2$), and Fermi motion at very high x ($x \gtrsim 0.2$). Understanding nPDFs is essential for interpreting results from high-energy nuclear collisions and probing the internal structure of nuclei at the partonic level.

Dijets are pairs of jets produced back-to-back in azimuth having a high probability of originating from the same hard scattering. Because of energy-momentum conservation, the back-to-back nature of dijets causes their production rates to be sensitive to lower-order ($2 \to 2$) partonic processes. Dijet production has previously been measured in proton-lead (pPb) collisions at the LHC [1–4]. In contrast to what has been observed in head-on lead-lead (PbPb) collisions, where interactions with the quark gluon plasma (QGP), such as QGP-induced gluon emissions, significantly alter the transverse momentum (p_{T}) balance between the jets of a dijet [5–8], no significant dijet p_{T} imbalance is observed in pPb data with respect to proton-proton (pp) distributions [2]. Moreover, measurements of inclusive jet [9–12] and inclusive charged-particle p_{T} spectra [13–15] also show no signs of jet modification at high p_{T} compared to pp data. The relatively small or negligible final-state effects in pPb collisions make jets reliable probes for nuclear PDF studies. Theoretical calculations have shown that the dijet pseudorapidity ($\eta^{\mathrm{dijet}} = (\eta_{\mathrm{jet}\,1} + \eta_{\mathrm{jet}\,2})/2$) distribution in pPb collisions can substantially constrain gluon nPDFs at low x [16–20] because of the small experimental and theoretical uncertainties [16].

The differences in parton distribution functions of free and bound nucleons are assessed by comparing experimental results to perturbative QCD (pQCD) calculations incorporating various nPDF sets. Discrepancies between experimental data and theoretical predictions are then used to refine the nPDF details. Global analyses combining data from different processes and experiments (e.g., deep inelastic scattering, Drell-Yan processes, and dijet production) are conducted to understand the nPDF comprehensively. Currently the key constraints of the gluon nPDF at low x ($<10^{-2}$) come from measurements of forward D^0 production in pPb collisions at $\sqrt{s_{\mathrm{NN}}} = 5.02$ TeV by the LHCb Collaboration [21], and from a previous CMS measurement of the η^{dijet} distributions in pPb collisions at $\sqrt{s_{\mathrm{NN}}} = 5.02$ TeV. Although the D^0 data are currently sensitive to lower x values, incorporation of these data into global fits also relies on the implementation of a charm quark fragmentation function. Dijet data do not have this drawback and provide important complementary information about the gluon nPDF, which should be a universal quantity regardless of the process used to probe it.

In this note, we present new measurements of η^{dijet} for multiple selections in dijet average transverse momentum, $p_{\mathrm{T}}^{\mathrm{ave}} = (p_{\mathrm{T},1} + p_{\mathrm{T},2})/2$, where $p_{\mathrm{T},1}$ is the p_{T} of the leading jet, and $p_{\mathrm{T},2}$ corresponds to the p_{T} of subleading jet of the dijet, measured in pPb collisions at $\sqrt{s_{\mathrm{NN}}} = 8.16$ TeV with the CMS detector at the LHC.

2 The CMS Detector

The central feature of the CMS apparatus is a superconducting solenoid of 6 m internal diameter, providing a magnetic field of 3.8 T. Within the solenoid volume, there are four primary subdetectors, including a silicon pixel and strip tracker detector, a lead tungstate crystal electromagnetic calorimeter, and a brass and scintillator hadron calorimeter, each composed of a barrel

and two endcap sections. Iron and quartz-fiber Cherenkov hadron forward (HF) calorimeters cover the range $3.0 < |\eta| < 5.2$. Muons are measured in the range $|\eta| < 2.4$ in gas-ionization detectors embedded in the steel flux-return yoke outside the solenoid, with detection planes made using three technologies: drift tubes, cathode strip chambers, and resistive-plate chambers. The silicon tracker measures charged particles within the range $|\eta| < 2.5$. For charged particles with $1 < p_T < 10\,\text{GeV}$ and $|\eta| < 1.4$, the track resolutions are typically 1.5% in p_T and 25–90 (45–150) μm in the transverse (longitudinal) impact parameter [22]. A detailed description of the CMS detector, together with a definition of the coordinate system used and the relevant kinematic variables, can be found in Ref. [23]. Events of interest are selected using a two-tiered trigger system: a hardware-based level-one trigger, and High-Level Trigger, which uses partial online event processing for relevant physics objects (such as jets, in this case) [24–26].

3 Data Sample and Event Selection

The present analysis uses pPb collision data recorded in 2016 at $\sqrt{s_{_{NN}}} = 8.16\,\text{TeV}$. The corresponding integrated luminosity of the sample is $174.6\,\text{nb}^{-1}$. The event reconstruction, event selections, and triggers are identical to those described in Refs. [27, 28]. A minimum-bias (MB) trigger [24] selects events in the lower part of the reported dijet p_T^{ave} range. This trigger requires an energy deposition in both HF sides or a track with $p_T > 0.4\,\text{GeV}$ in the pixel detector. In addition, triggers examining anti-k_T jets [29, 30] with a radius parameter of $R = 0.4$ reconstructed with an online version of the particle flow algorithm are used to enhance the statistical significance of the measurements at high p_T^{ave} values. The jet p_T thresholds for these triggers were 60, 80, and 100 GeV.

Events are required to have at least one interaction vertex, reconstructed from two or more tracks, with a distance $|v_z| < 15\,\text{cm}$ from the center of the nominal interaction point along the beam axis. Additionally, events must have at least one calorimeter tower with energy above 3 GeV in at least one HF calorimeter, removing approximately 99% of the background caused by ultraperipheral events and electromagnetic contamination. Filters are additionally applied to exclude events with multiple interactions per bunch crossing (pileup) [27, 28].

Due to the different energies of the proton (6.5 TeV) and lead (2.56 TeV per nucleon) beams, the nucleon-nucleon center-of-mass frame experiences a boost in the detector reference frame. During a part of the data-taking period, the proton and lead beam directions were reversed. For the data set collected with the proton beam in the opposite direction, the sign of the standard CMS definition of η was inverted, ensuring the proton beam always moved towards positive η. Consequently, a massless particle emitted at $\eta_{CM} = 0$ in the center-of-mass frame will be detected at $\eta_{lab} = +0.465$ in the laboratory frame. The η^{dijet} distributions described in this note are presented using the η_{lab} value defined using the laboratory reference frame, while, in order to avoid acceptance effects, the forward-to-backward analysis is performed using the center-of-mass frame inclusive jet frame η_{CM}.

Monte Carlo (MC) simulations are employed to determine the jet performance, determine event selections, perform cross-checks, and to account for other potential detector effects. Events generated with the PYTHIA 8+EPOS [31] event generators are used for this purpose. Furthermore, GEANT4 [32] is utilized for full detector simulation in the event reconstruction.

The present analysis reconstructs jets using the CMS "particle flow" algorithm [33, 34]. The particle flow algorithm identifies all stable particles in an event and classifies them into categories such as neutral hadrons, electrons, muons, and photons, utilizing information from all

sub-detectors. These particle flow objects are combined into pseudo-towers. The transverse energy of a pseudo-tower is calculated as the scalar sum of the transverse energy of the particle flow objects, with the assumption of zero mass.

Jets are then reconstructed from the pseudo-towers using the anti-k_{T} sequential recombination algorithm provided in the FASTJET framework [30]. A distance parameter of $R = 0.4$ is used for the jet reconstruction. Once the jets are reconstructed, jet energy corrections derived from MC simulations are applied to correct for detector effects and avoid misreconstructed jets. Jets consisting of a single track with a maximum track p_{T} exceeding 98% of the jet p_{T}, or with a large number of tracks having a maximum track p_{T} being less than 1% of the jet p_{T}, are removed from the analysis.

To form a dijet, all jets in the range $|\eta| < 5$ are searched and the jets having the highest (leading jet) and second-highest (subleading jet) p_{T} are identified in the event. After the identification of the dijet, events are only kept for further analysis if the following conditions are met: the leading jet and subleading jet must have $p_{\mathrm{T}} > 50\,\mathrm{GeV}$ and $p_{\mathrm{T}} > 40\,\mathrm{GeV}$, respectively; the leading and subleading jets must fall within the range $|\eta| < 3$; and the two jets must have a difference in azimuthal angle that is $>5\pi/6$ radians, i.e., they must be approximately back-to-back in azimuth. Note that these selections enforce that there is a maximum of one dijet per event. Dijets passing all these criteria are then classified based on their $p_{\mathrm{T}}^{\mathrm{ave}}$. This analysis studies dijets in the range $50 < p_{\mathrm{T}}^{\mathrm{ave}} < 500\,\mathrm{GeV}$. The η^{dijet} distribution is then studied for a given $p_{\mathrm{T}}^{\mathrm{ave}}$ selection.

4 Systematic Uncertainties

The systematic uncertainty in the measured distributions related to the jet energy scale (JES) is significant since the width of the η^{dijet} distribution decreases with increasing $p_{\mathrm{T}}^{\mathrm{ave}}$ [2]. Studies with dijet and γ + jet events [35] show that the JES in data can deviate from that in simulated events by up to 3% at $\eta^{\mathrm{dijet}} = 0$ and up to 10% at forward/backward pseudorapidities. To evaluate the corresponding uncertainties, the JES is shifted by $\pm 2\%$ for data, and the deviations of the observed pseudorapidity spectra are taken as systematic uncertainties. To account for uncertainties related to jet p_{T} (pointing) resolution, the differences between the η^{dijet} spectra obtained from detector-level, i.e., reconstructed jet p_{T} (η) and generator-level jet p_{T} (η) with PYTHIA 8 events embedded into simulated pPb underlying events (PYTHIA 8+EPOS) are quoted as systematic uncertainties. To model the underlying event (UE) in pPb collisions, minimum bias pPb events are simulated using the EPOS event generator [31]. The systematic uncertainty related to the presence of the UE is below 1%. The uncertainty in the accuracy of η^{dijet} reconstruction for each $p_{\mathrm{T}}^{\mathrm{ave}}$ selection is found to be in the range from 0.5% to 3%. The systematic uncertainty due to pileup was found to be small (below 1%). The total systematic uncertainty for the measurement is calculated by summing up all the individual contributions in a quadrature.

5 Results

The differential dijet pseudorapidity, η^{dijet}, distributions are shown in Figs. 1 and 2 for sixteen $p_{\mathrm{T}}^{\mathrm{ave}}$ selections spanning the range from 50–500 GeV. The distributions are normalized by the total number of dijets in the $p_{\mathrm{T}}^{\mathrm{ave}}$ selection. The results are plotting against the η^{dijet} value calculated in the laboratory reference frame. Statistical uncertainties are represented by error bars, and are smaller than the marker size in many cases. Systematic uncertainties are represented by shaded areas. In general, the data show a peak around $\eta^{\mathrm{dijet}} \approx 0$. The η^{dijet} distribution

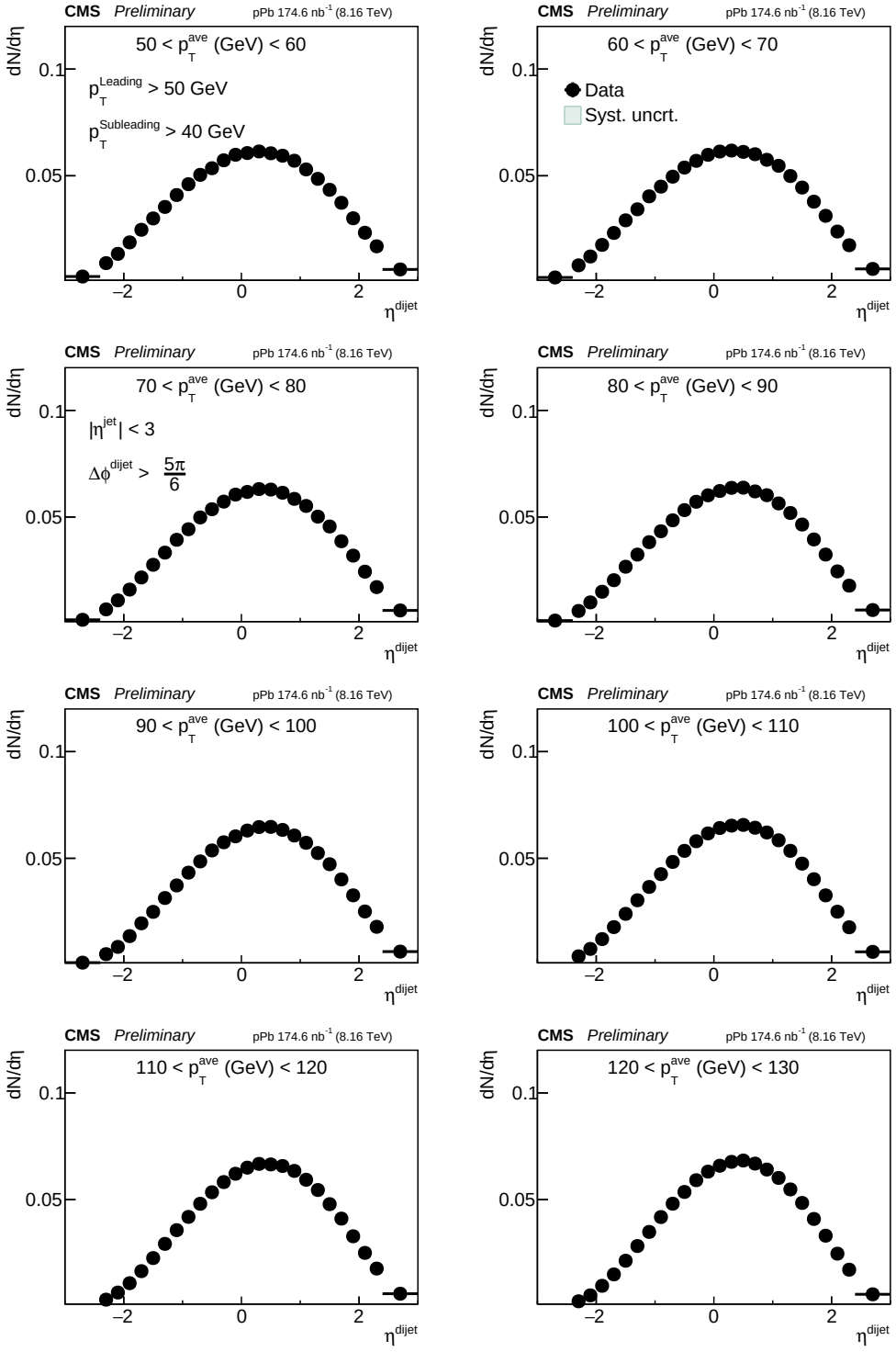

Figure 1: Measured η^{dijet} distributions in different bins of the dijet average transverse momentum, $p_{\text{T}}^{\text{ave}}$. The shaded areas represent the systematic uncertainties, and the error bars show the statistical uncertainties.

becomes narrower with increasing $p_{\text{T}}^{\text{ave}}$, and the corresponding average Q^2 of the hard process producing the dijet, providing a more differential scan of the interaction scale.

Similar qualitative behavior was also observed in the previous CMS analysis of η^{dijet} distri-

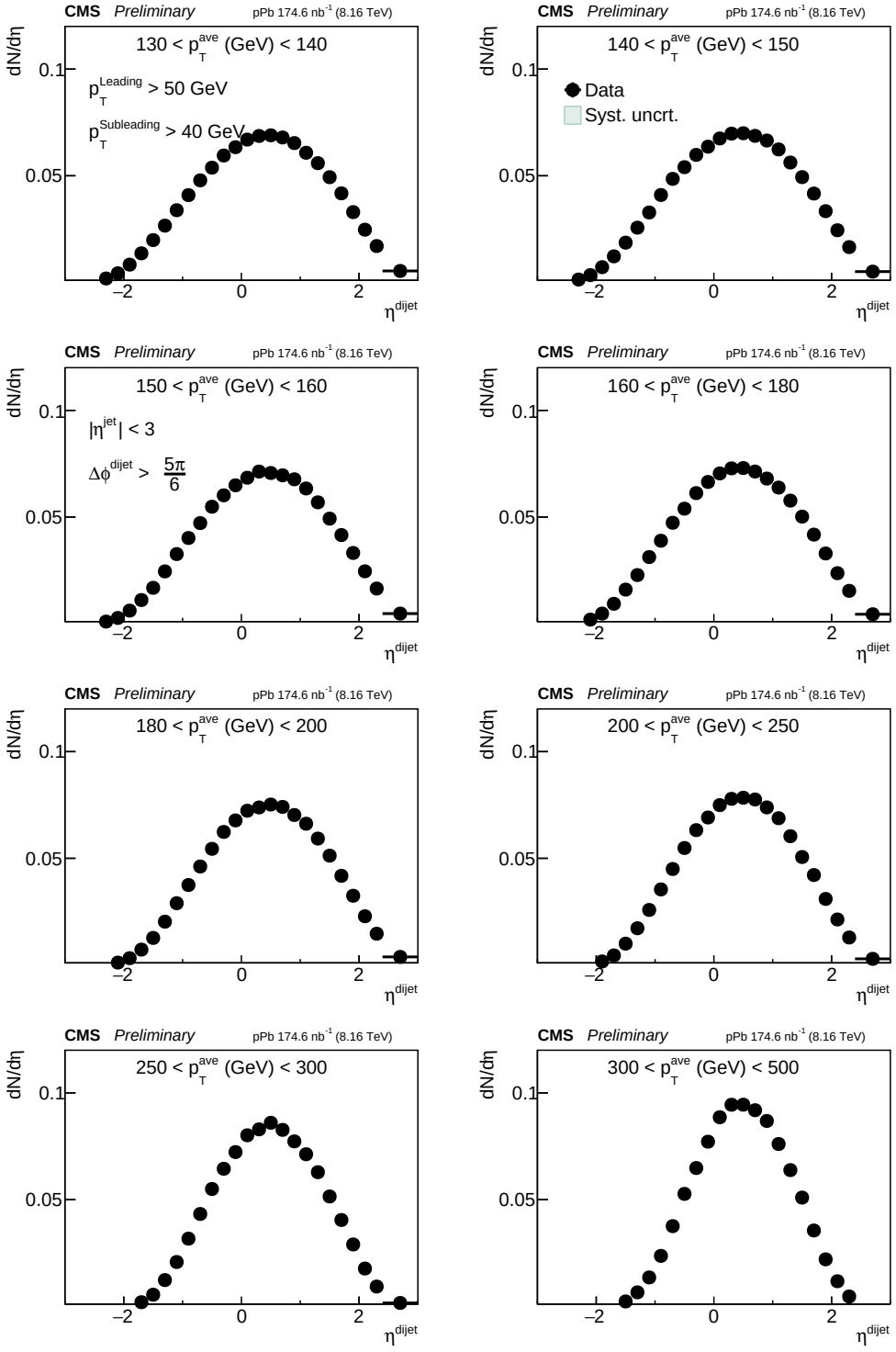

Figure 2: Measured η^{dijet} distributions in different bins of the dijet average transverse momentum, $p_{\text{T}}^{\text{ave}}$. The shaded areas represent the systematic uncertainties, and the error bars show the statistical uncertainties.

butions at $\sqrt{s_{\text{NN}}} = 5.02\,\text{TeV}$ [1]. The new data provide a significantly more differential scan in $p_{\text{T}}^{\text{ave}}$, and therefore the scale of the interaction and the structure of the probed system, when compared to the previous CMS measurement. Although the overall range of η^{dijet} and $p_{\text{T}}^{\text{ave}}$ covered is similar between the two measurements, the average x probed in a given $(p_{\text{T}}^{\text{ave}}, \eta^{\text{dijet}})$ bin

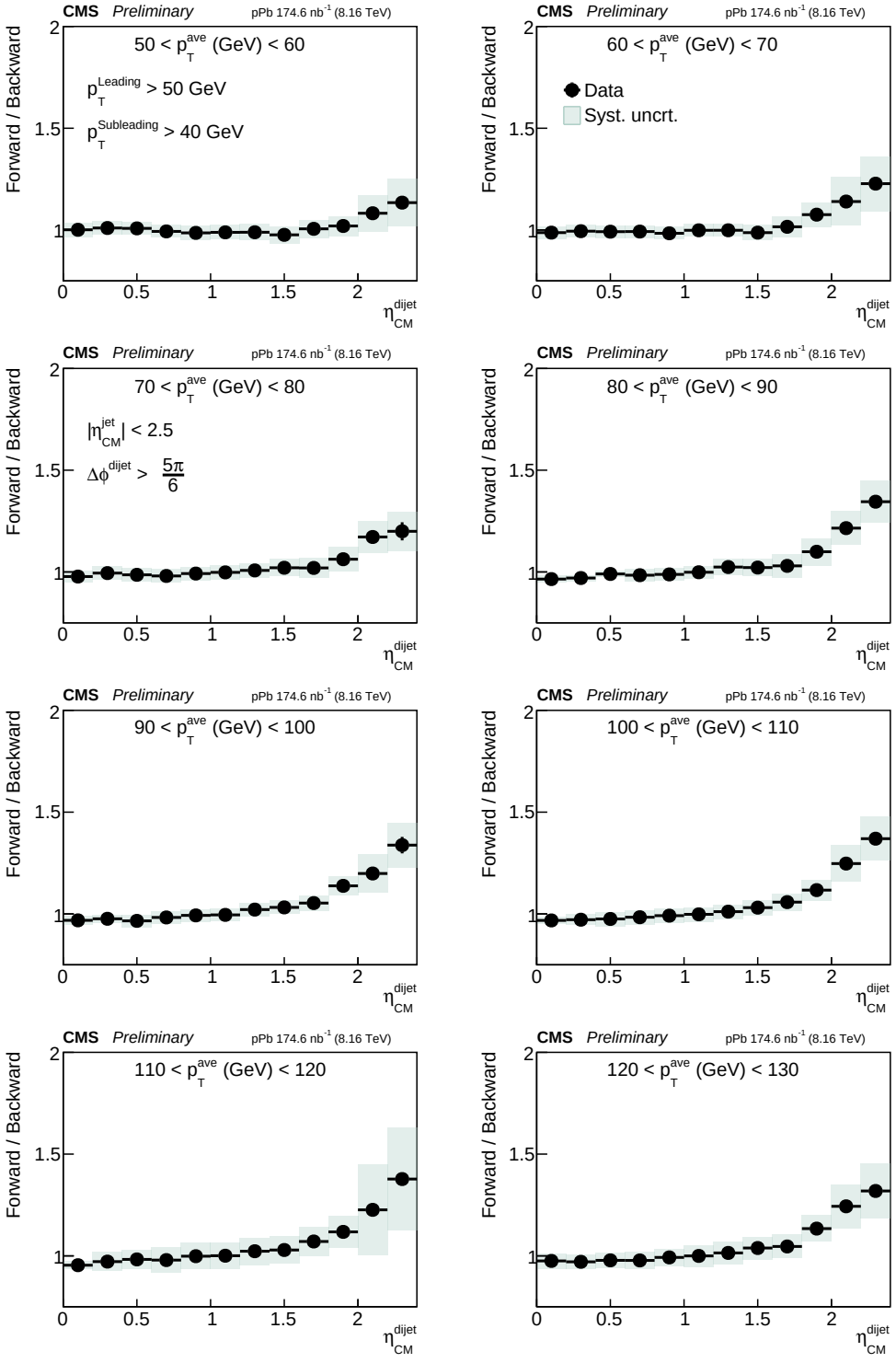

Figure 3: Measured forward-to-backward $\eta_{\mathrm{CM}}^{\mathrm{dijet}}$ ratios in different bins of $p_{\mathrm{T}}^{\mathrm{ave}}$. The shaded areas represent the systematic uncertainties, and the error bars show the statistical uncertainties.

scales with the inverse of $\sqrt{s_{\mathrm{NN}}}$. Thus, this measurement performed for collisions at 8.16 TeV probes x values that are approximately 40% lower than the previous measurement at 5.02 TeV, significantly extending the low-x range in which global nPDF fits can be performed for this observable.

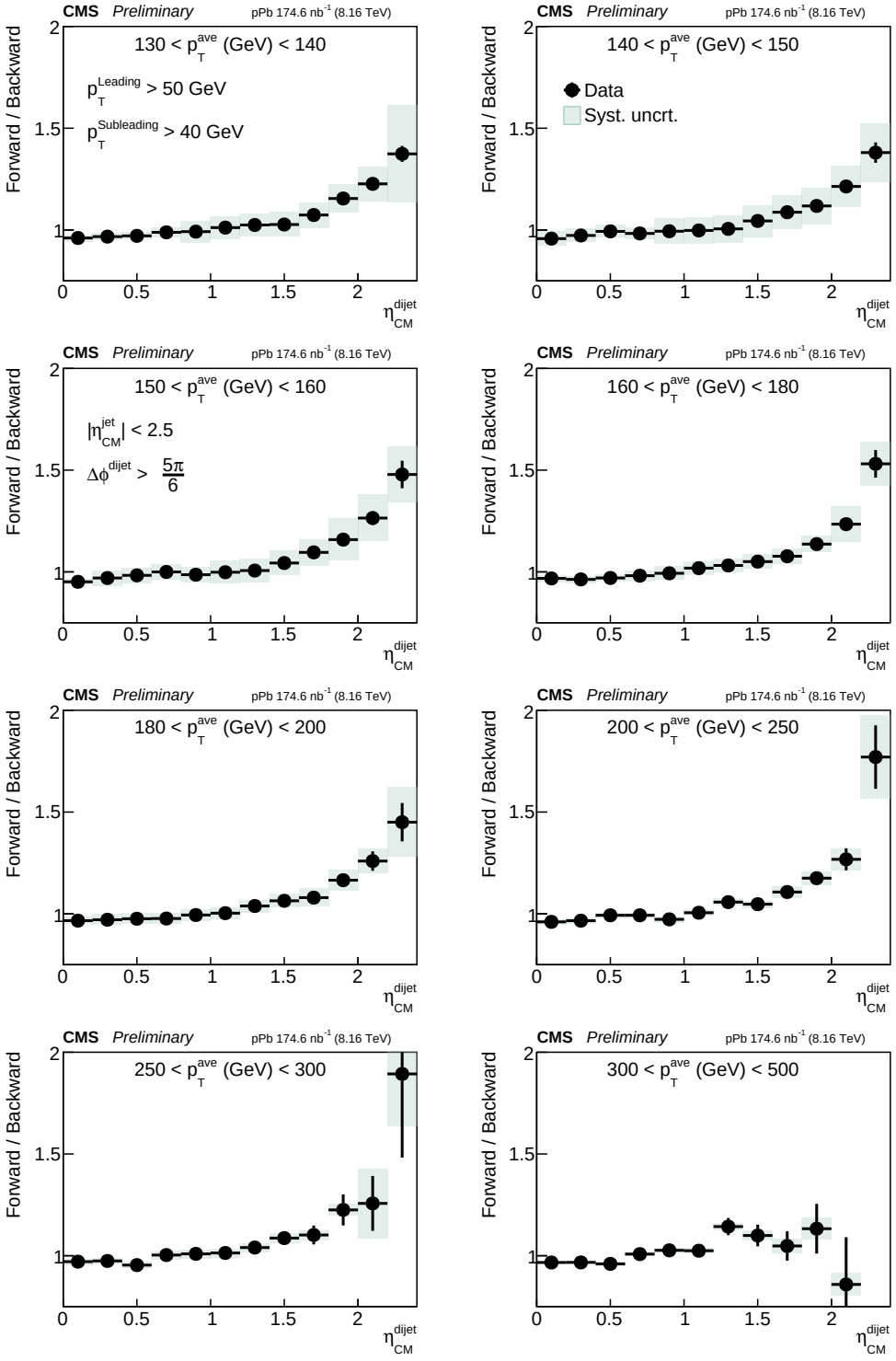

Figure 4: Measured forward-to-backward $\eta_{\mathrm{CM}}^{\mathrm{dijet}}$ ratios in different bins of $p_{\mathrm{T}}^{\mathrm{ave}}$. The shaded areas represent the systematic uncertainties, and the error bars show the statistical uncertainties.

In the absence of a proton-proton reference at the same collision energy as pPb, forward-to-backward ratios of the η^{dijet} distributions are constructed. By comparing dijet yields in the forward ($\eta_{\mathrm{CM}}^{\mathrm{dijet}} > 0$) and backward ($\eta_{\mathrm{CM}}^{\mathrm{dijet}} < 0$) pseudorapidity regions, these ratios help to isolate asymmetries that may arise due to nuclear modifications. Forward pseudorapidities cor-

respond to lower values of the Bjorken x and lie within the shadowing region. Similarly, central and backward pseudorapidities correspond to the antishadowing and EMC effect regions. Forward-to-backward ratios are particularly useful because they inherently cancel out many systematic uncertainties which affect the forward and backward regions equally. In this analysis, to avoid acceptance effects, the forward-to-backward ratios are calculated in the center-of-mass frame, with inclusive jets selected in the pseudorapidity range $|\eta_{\mathrm{CM}}| < 2.5$. Other event selection and kinematic cuts remain the same. Figures 3 and 4 show the forward-to-backward ratios of the η^{dijet} distributions for the same $p_{\mathrm{T}}^{\mathrm{ave}}$ selections as in Figs. 1 and 2. The ratios demonstrate deviations from unity at $\eta_{\mathrm{CM}}^{\mathrm{dijet}} > 1.2$, indicating the presence of nPDF effects.

6 Summary

In summary, we report measurements of the dijet pseudorapidity, η^{dijet}, across various average transverse momentum intervals, $p_{\mathrm{T}}^{\mathrm{ave}}$, intervals in pPb collisions at a nucleon-nucleon center-of-mass energy of $\sqrt{s_{\mathrm{NN}}} = 8.16\,\mathrm{TeV}$. The measured distributions can be compared to theoretical calculations performed with nuclear parton distribution functions (nPDFs). This dataset explores lower Bjorken x values compared to prior dijet analyses, thereby accessing a previously unconstrained region of the gluon nPDF via dijet final states. It establishes new constraints on existing nPDF models, crucial for advancing our understanding of high-p_{T} and high-mass particle production at the LHC energies.

Acknowledgments

References

[1] CMS Collaboration, "Constraining gluon distributions in nuclei using dijets in proton-proton and proton-lead collisions at $\sqrt{s_{\mathrm{NN}}} = 5.02\,\mathrm{TeV}$", *Phys. Rev. Lett.* **121** (2018) 062002, doi:10.1103/PhysRevLett.121.062002.

[2] CMS Collaboration, "Studies of dijet transverse momentum balance and pseudorapidity distributions in ppb collisions at $\sqrt{s_{\mathrm{NN}}} = 5.02\,\mathrm{TeV}$", *Eur. Phys. J. C* **74** (2014) 2951, doi:10.1140/epjc/s10052-014-2951-y, arXiv:1401.4433.

[3] ALICE Collaboration, "Measurement of dijet k_T in p-pb collisions at $\sqrt{s_{\mathrm{NN}}} = 5.02\,\mathrm{TeV}$", *Phys. Lett. B* **746** (2015) 385, doi:10.1016/j.physletb.2015.05.033, arXiv:1503.03050.

[4] CMS Collaboration, "Overview of high-density QCD studies with the CMS experiment at the LHC", 2024. arXiv:2405.10785. Submitted to *Phys. Rep.*

[5] CMS Collaboration, "Observation and studies of jet quenching in pbpb collisions at nucleon-nucleon center-of-mass energy $\sqrt{s_{\mathrm{NN}}} = 2.76\,\mathrm{TeV}$", *Phys. Rev. C* **84** (2011) 024906, doi:10.1103/PhysRevC.84.024906, arXiv:1102.1957.

[6] ATLAS Collaboration, "Observation of a centrality-dependent dijet asymmetry in lead-lead collisions at $\sqrt{s_{\mathrm{NN}}} = 2.76\,\mathrm{TeV}$ with the ATLAS detector at the LHC", *Phys. Rev. Lett.* **105** (2010) 252303, doi:10.1103/PhysRevLett.105.252303, arXiv:1011.6182.

[7] CMS Collaboration, "Jet momentum dependence of jet quenching in pbpb collisions at $\sqrt{s_{\mathrm{NN}}} = 2.76\,\mathrm{TeV}$", *Phys. Lett. B* **712** (2012) 176, doi:10.1016/j.physletb.2012.04.058, arXiv:1202.5022.

[8] CMS Collaboration, "Measurement of transverse momentum relative to dijet systems in pbpb and pp collisions at $\sqrt{s_{\mathrm{NN}}} = 2.76\,\mathrm{TeV}$", *JHEP* **01** (2016) 006, doi:10.1007/JHEP01(2016)006, arXiv:1509.09029.

[9] ATLAS Collaboration, "Centrality and rapidity dependence of inclusive jet production in $\sqrt{s_{\mathrm{NN}}} = 5.02\,\mathrm{TeV}$ proton-lead collisions with the ATLAS detector", *Phys. Lett. B* **748** (2015) 392, doi:10.1016/j.physletb.2015.07.023, arXiv:1412.4092.

[10] ALICE Collaboration, "Measurement of charged jet production cross sections and nuclear modification in p-pb collisions at $\sqrt{s_{\mathrm{NN}}} = 5.02\,\mathrm{TeV}$", *Phys. Lett. B* **749** (2015) 68, doi:10.1016/j.physletb.2015.07.054, arXiv:1503.00681.

[11] CMS Collaboration, "Transverse momentum spectra of inclusive b jets in ppb collisions at $\sqrt{s_{\mathrm{NN}}} = 5.02\,\mathrm{TeV}$", *Phys. Lett. B* **754** (2016) 59, doi:10.1016/j.physletb.2016.01.010, arXiv:1510.03373.

[12] CMS Collaboration, "Measurement of inclusive jet production and nuclear modifications in ppb collisions at $\sqrt{s_{\mathrm{NN}}} = 5.02\,\mathrm{TeV}$", *Eur. Phys. J. C* **76** (2016) 372, doi:10.1140/epjc/s10052-016-4205-7, arXiv:1601.02001.

[13] ALICE Collaboration, "Transverse momentum dependence of inclusive primary charged-particle production in p-pb collisions at $\sqrt{s_{\mathrm{NN}}} = 5.02\,\mathrm{TeV}$", *Eur. Phys. J. C* **74** (2014) 3054, doi:10.1140/epjc/s10052-014-3054-5, arXiv:1405.2737.

[14] CMS Collaboration, "Nuclear effects on the transverse momentum spectra of charged particles in ppb collisions at $\sqrt{s_{\mathrm{NN}}} = 5.02\,\mathrm{TeV}$", *Eur. Phys. J. C* **75** (2015) 237, doi:10.1140/epjc/s10052-015-3435-4, arXiv:1502.05387.

[15] CMS Collaboration, "Study of B meson production in pPb collisions at $\sqrt{s_{\mathrm{NN}}} = 5.02\,\mathrm{TeV}$ using exclusive hadronic decays", *Phys. Rev. Lett.* **116** (2016) 032301, doi:10.1103/PhysRevLett.116.032301, arXiv:1508.06678.

[16] K. J. Eskola, H. Paukkunen, and C. A. Salgado, "A perturbative qcd study of dijets in p+pb collisions at the LHC", *JHEP* **10** (2013) 213, doi:10.1007/JHEP10(2013)213, arXiv:1308.6733.

[17] H. Paukkunen, K. J. Eskola, and C. Salgado, "Dijets in p+pb collisions and their quantitative constraints for nuclear pdfs", *Nucl. Phys. A* **931** (2014) 331, doi:10.1016/j.nuclphysa.2014.07.012, arXiv:1408.4563.

[18] N. Armesto et al., "An analysis of the impact of lhc run i proton-lead data on nuclear parton densities", *Eur. Phys. J. C* **76** (2016) 218, doi:10.1140/epjc/s10052-016-4078-9, arXiv:1512.01528.

[19] H. Khanpour and S. Atashbar Tehrani, "Global analysis of nuclear parton distribution functions and their uncertainties at next-to-next-to-leading order", *Phys. Rev. D* **93** (2016) 014026, doi:10.1103/PhysRevD.93.014026, arXiv:1601.00939.

[20] L. Apolinrio, Y.-J. Lee, and M. Winn, "Heavy quarks and jets as probes of the QGP", *Prog. Part. Nucl. Phys.* **127** (2022) 103990, doi:https://doi.org/10.1016/j.ppnp.2022.103990.

[21] LHCb Collaboration, "Study of prompt D^0 meson production in $p$pb collisions at $\sqrt{s_{NN}} = 5$ TeV", *JHEP* **10** (2017) 090, doi:10.1007/JHEP10(2017)090, arXiv:1707.02750.

[22] CMS Collaboration, "Description and performance of track and primary-vertex reconstruction with the cms tracker", *JINST* **9** (2014) P10009, doi:10.1088/1748-0221/9/10/P10009, arXiv:1405.6569.

[23] CMS Collaboration, "The CMS experiment at the CERN LHC", *JINST* **3** (2008) S08004, doi:10.1088/1748-0221/3/08/S08004.

[24] CMS Collaboration, "Dependence on pseudorapidity and centrality of charged hadron production in pbpb collisions at a nucleon-nucleon centre-of-mass energy of 2.76 TeV", *JHEP* **08** (2011) 141, doi:10.1007/JHEP08(2011)141, arXiv:1107.4800.

[25] CMS Collaboration, "Performance of the CMS level-1 trigger in proton-proton collisions at $\sqrt{s} = 13$ TeV", *JINST* **15** (2020) P10017, doi:10.1088/1748-0221/15/10/P10017, arXiv:2006.10165.

[26] CMS Collaboration, "The CMS trigger system", *JINST* **12** (2017) P01020, doi:10.1088/1748-0221/12/01/P01020, arXiv:1609.02366.

[27] CMS Collaboration, "Constraints on the chiral magnetic effect using charge-dependent azimuthal correlations in pPb and pbpb collisions at the CERN large hadron collider", *Phys. Rev. C* **97** (2018) 044912, doi:10.1103/PhysRevC.97.044912, arXiv:1708.01602.

[28] CMS Collaboration, "Observation of correlated azimuthal anisotropy fourier harmonics in pp and pPb collisions at the LHC", *Phys. Rev. Lett.* **120** (2018) 092301, doi:10.1103/PhysRevLett.120.092301, arXiv:1709.09189.

[29] M. Cacciari, G. P. Salam, and G. Soyez, "The anti-k_T jet clustering algorithm", *JHEP* **04** (2008) 063, doi:10.1088/1126-6708/2008/04/063, arXiv:0802.1189.

[30] M. Cacciari, G. P. Salam, and G. Soyez, "FastJet user manual", *Eur. Phys. J. C* **72** (2012) 1896, doi:10.1140/epjc/s10052-012-1896-2, arXiv:1111.6097.

[31] T. Pierog et al., "EPOS LHC: Test of collective hadronization with data measured at the CERN large hadron collider", *Phys. Rev. C* **92** (2015) 034906, doi:10.1103/PhysRevC.92.034906.

[32] GEANT4 Collaboration, "GEANT4–a simulation toolkit", *Nucl. Instrum. Meth. A* **506** (2003) 250, doi:10.1016/S0168-9002(03)01368-8.

[33] CMS Collaboration, "Particle-flow event reconstruction in CMS and performance for jets, taus, and met", Technical Report CMS-PAS-PFT-09-001, 2009.

[34] CMS Collaboration, "Commissioning of the particle-flow event reconstruction with the first LHC collisions recorded in the CMS detector", Technical Report CMS-PAS-PFT-10-001, 2010.

[35] CMS Collaboration, "Determination of jet energy calibration and transverse momentum resolution in CMS", *JINST* **6** (2011) P11002, doi:10.1088/1748-0221/6/11/P11002, arXiv:1107.4277.